International Communications in Heat and Mass Transfer 38 (2011) 1392–1399

Contents lists available at ScienceDirect

International Communications in Heat and Mass Transfer

journal homepage: www.elsevier.com/locate/ichmt

Numerical heat transfer study of turbulent square-duct flow through inline V-shaped discrete ribs ☆

Pongjet Promvonge *, Wayo Changcharoen, Sutapat Kwankaomeng, Chinaruk Thianpong

Department of Mechanical Engineering, Faculty of Engineering, King Mongkut's Institute of Technology Ladkrabang, Bangkok 10520, Thailand

ARTICLE INFO

Available online 9 August 2011

Keywords:
Periodic flow
Square duct
Turbulent flow
Heat transfer
V-discrete rib

ABSTRACT

A numerical work has been conducted to examine turbulent periodic flow and heat transfer characteristics in a three dimensional square-duct with inline 60° V-shaped discrete thin ribs placed on two opposite heated walls. The isothermal-flux condition is applied only to the upper and lower duct walls while the two sidewalls are insulated, similar to internal passage cooling of gas turbine blades. The computations are based on the finite volume method with the SIMPLE algorithm for handling the pressure–velocity coupling. Air is the working fluid with the flow rate in terms of Reynolds numbers ranging from 10,000 to 25,000. The numerical result is validated with available square-rib measured data and found to agree well with measurement. The computation reveals that the ribbed duct flow is fully developed periodic flow and heat transfer profiles at about $x/D = 7$–11 downstream of the inlet. Effects of different rib height to duct diameter ratios, *BR*, on thermal characteristics for a periodic ribbed duct flow are investigated. It is found that a pair of counter-rotating vortices (P-vortex) caused by the rib can induce impingement/attachment flows on the walls leading to greater increase in heat transfer over the test duct. In addition, the rise of *BR* values leads to the increase in heat transfer and friction loss. The maximum thermal performance is around 1.8 for the rib with $BR = 0.0725$ where the heat transfer rate is about 4.0 times above the smooth duct at lower Reynolds number.

1. Introduction

In the design of modern aircraft engines, high thrust–weight ratio and low fuel consumption rate are needed and used as the key criteria for the design. The way to achieve the higher thrust–weight ratio of aircrafts is to improve the thermal efficiency of turbine. To reach this purpose, an effective way is to increase the turbine inlet temperature. However, to avoid the melting point of the turbine blade material, internal cooling of the gas turbine blades is required for the gas turbine operation.

Several techniques have been developed to enhance the heat transfer in internal duct cooling of the gas turbine blades. Ribs have been widely used in the design of gas turbine blades of aircraft engines. Many investigations have been conducted to examine the heat transfer enhancement in ribbed ducts. Webb et al. [1] presented the heat transfer and friction behaviors in ducts with internal repeated ribs. Han et al. [2] studied on pressure drop and heat transfer in a square channel with several rib configurations at $p/e = 10$ and $e/D = 0.0625$ on two walls and found that the 45° angled and 60° V-shaped ribs provide higher heat transfer than the 90° transverse ribs. The heat transfer and the friction factor were highest for the 60° compared to 45° and 90° amongst the angled and V-shaped ribs. Lau et al. [3] examined the turbulent heat transfer characteristics in a square channel with various V-shaped ribs and presented that the 60° V-shaped ribs with $P/e = 10$ provides the highest thermal performance. Han and Zhang [4] investigated the heat transfer enhancement in a square channel with 60° V-broken ribs on two opposite walls and observed that the rib with $e/D = 0.0625$ and $p/e = 10$ provides higher heat transfer and performs better than the continuous rib. Chandra et al. [5] reported thermal behaviors in a square channel with continuous ribs on one, two, three and four walls and observed that the heat transfer and friction factor increase with the rise in the number of ribbed walls. Promvonge and Thianpong [6] studied the effect of various rib shapes: wedge, triangular and rectangular ribs on thermal behaviors in a channel and showed that the staggered triangular rib performs the best.

Tanda [7] studied the thermal and flow behaviors in a channel with V-shaped continuous and broken ribs and found that the V-broken ribs give higher thermal performance than the continuous ribs. Won and Ligrani [8] carried out experimentally a comparison of heat transfer characteristics of channels with 45° parallel or crossed ribs and found that the 45° parallel ribs perform better than the 45° crossed ribs. SriHarsha et al. [9] also provided local and average heat transfer in a square duct with 90° continuous and 60° V-broken ribs on two opposite heated walls and found that the V-broken rib gives much higher thermal performance than the continuous rib. Effects of 60° V-shaped baffles on thermal and friction characteristics in a channel were reported by Promvonge [10]. Gupta et al. [11] examined the local heat transfer distributions in a square channel with continuous, profiled and broken ribs and reported that the heat transfer from the V-broken ribs is higher

☆ Communicated by W.J. Minkowycz.

* Corresponding author.
E-mail address: kppongje@kmitl.ac.th (P. Promvonge).

0735-1933/$ – see front matter © 2011 Elsevier Ltd. All rights reserved.
doi:10.1016/j.icheatmasstransfer.2011.07.014

Nomenclature

A	convection heat transfer area, m^2
BR	blockage ratio, (e/D)
D	hydraulic diameter of square duct, $(=H)$
e	rib height, m
f	friction factor
H	duct height, m
h	convective heat transfer coefficient, $W\,m^{-2}\,K^{-1}$
k	turbulent kinetic energy, $(k=\frac{1}{2}\overline{u_i'u_i'})$
k_a	thermal conductivity of air, $W\,m^{-1}\,K^{-1}$
L	duct length, m
Nu	Nusselt number
p	rib pitch spacing or cyclic length of one module, m
P	static pressure, Pa
Pr	Prandtl number
PR	pitch spacing ratio, p/D
Re	Reynolds number, $(\rho u_0 D/\mu)$
T	temperature, K
TEF	thermal performance enhancement factor, $(Nu/Nu_0)/(f/f_0)^{1/3}$
u_i	velocity component in x_i-direction, $m\,s^{-1}$
u_i'	fluctuation velocity in x_i-direction, $m\,s^{-1}$
u_0	mean or uniform velocity in smooth duct, $m\,s^{-1}$
s	rib thickness, m
x	coordinate direction

Greek letter

μ	dynamic viscosity, $kg\,s^{-1}\,m^{-1}$
Γ	thermal diffusivity
ε	dissipation rate
α	angle of attack, degree
ρ	density, $kg\,m^{-3}$

Subscript

in	inlet
0	smooth duct
w	wall
pp	pumping power

than that of the continuous and profiled ribs. Tatsumi et al. [12] numerically studied thermal behaviors in turbulent square-duct flow through oblique discrete ribs mounted on one wall and found that considerable heat transfer enhancement is obtained due to a stronger secondary flow motion. Yang and Hwang [13] examined numerically heat transfer characteristics in a rectangular duct with slit and solid ribs on one wall and reported that the slit rib performed better than the solid one. Kim and Lee [14] presented a numerical optimization procedure for design of a square channel with V-shaped square ribs extruded on both walls to enhance turbulent heat transfer. In addition, influences of various angled continuous baffles (or thin ribs) placed on two walls of a square duct on heat transfer and flow characteristics were investigated numerically [15–17]. The investigations revealed that the streamwise vortex flows caused by the angled baffles existed and helped to induce impingement jets on the duct walls leading to drastic increase in heat transfer rate.

Most of the investigations, cited above, have focused on heat transfer characteristics for rib height and spacing ratios for transverse, angled, V-shaped, continuous or broken, square ribs. The study on turbulent periodic flows through V-discrete ribs in a square duct has rarely been reported, especially for numerical work. In the present work, the numerical computations for 3D turbulent periodic flows over the 60° V-discrete thin ribs mounted repeatedly on two opposite heated walls of a square duct are conducted with the main aim being to examine the changes in the flow structure and heat transfer characteristics.

2. Flow configuration

The flow system of interest is a horizontal square duct with V-broken (or discrete) ribs repeatedly placed on the upper and lower duct walls as depicted in Fig. 1. The duct is divided into 3 sections: entry (0.32 m), test section (0.575 m) and exit (0.055 m). The details of the full length ribbed duct in Fig. 1a are all similar to the ribbed duct of SriHarsha et al. [9] where a module of periodic flow duct showing its plan view and dimensions is depicted in Fig. 1b. The computational domain and grids in quarter module only due to symmetry is presented in Fig. 1c. The periodic flow under consideration attained a fully developed periodic flow and thermal condition where the velocity field and heat transfer pattern repeats itself from one module to another. In the flow module, the air enters the duct at an inlet temperature, $T_{in}=300$ K and flows over the inline 60° V-discrete ribs where e and s are the rib height and thickness, respectively. All the square rib size and location on the duct module are similar to Ref. [9] with the rib cross section of 0.0025×0.0025 m while the thin rib is set to $s/D=0.0125$. The duct height, H is 0.04 m and e/D is known as the blockage ratio, BR. The axial pitch or spacing between the ribs is set to p in which p/D is defined as the rib pitch ratio, $PR=0.625$. To investigate an effect of the thin rib height, the blockage ratio is varied in a range of $BR=0.025$–0.125 in the current computation.

3. Mathematical modeling

The numerical model for fluid flow and heat transfer in the square duct is developed under the following assumptions:

- Steady three-dimensional flow and heat transfer.
- The flow is periodic, fully developed, turbulent and incompressible.
- Constant fluid properties.
- Body forces, viscous dissipation and radiation heat transfer are ignored.

Based on the above assumptions, the duct flow is governed by the Reynolds averaged Navier–Stokes (RANS) equations and the energy equation. In the Cartesian tensor system these equations can be written as follows:

Continuity equation:

$$\frac{\partial}{\partial x_i}(\rho u_i)=0 \tag{1}$$

Momentum equation:

$$\frac{\partial}{\partial x_j}\left(\rho u_i u_j\right)=-\frac{\partial P}{\partial x_i}+\frac{\partial}{\partial x_j}\left[\mu\left(\frac{\partial u_i}{\partial x_j}-\rho\overline{u_i'u_j'}\right)\right] \tag{2}$$

where ρ is the density of fluid, and u_i is a mean component of velocity in the direction x_i, P is the pressure, μ is the dynamic viscosity, and u' is a fluctuating component of velocity. Repeated indices indicate summation from one to three for 3-dimensional problems.

Energy equation:

$$\frac{\partial}{\partial x_i}(\rho u_i T)=\frac{\partial}{\partial x_j}\left((\Gamma+\Gamma_t)\frac{\partial T}{\partial x_j}\right) \tag{3}$$

where Γ and Γ_t are molecular thermal diffusivity and turbulent thermal diffusivity, respectively and are given by

$$\Gamma=\mu/Pr \text{ and } \Gamma_t=\mu_t/Pr_t. \tag{4}$$

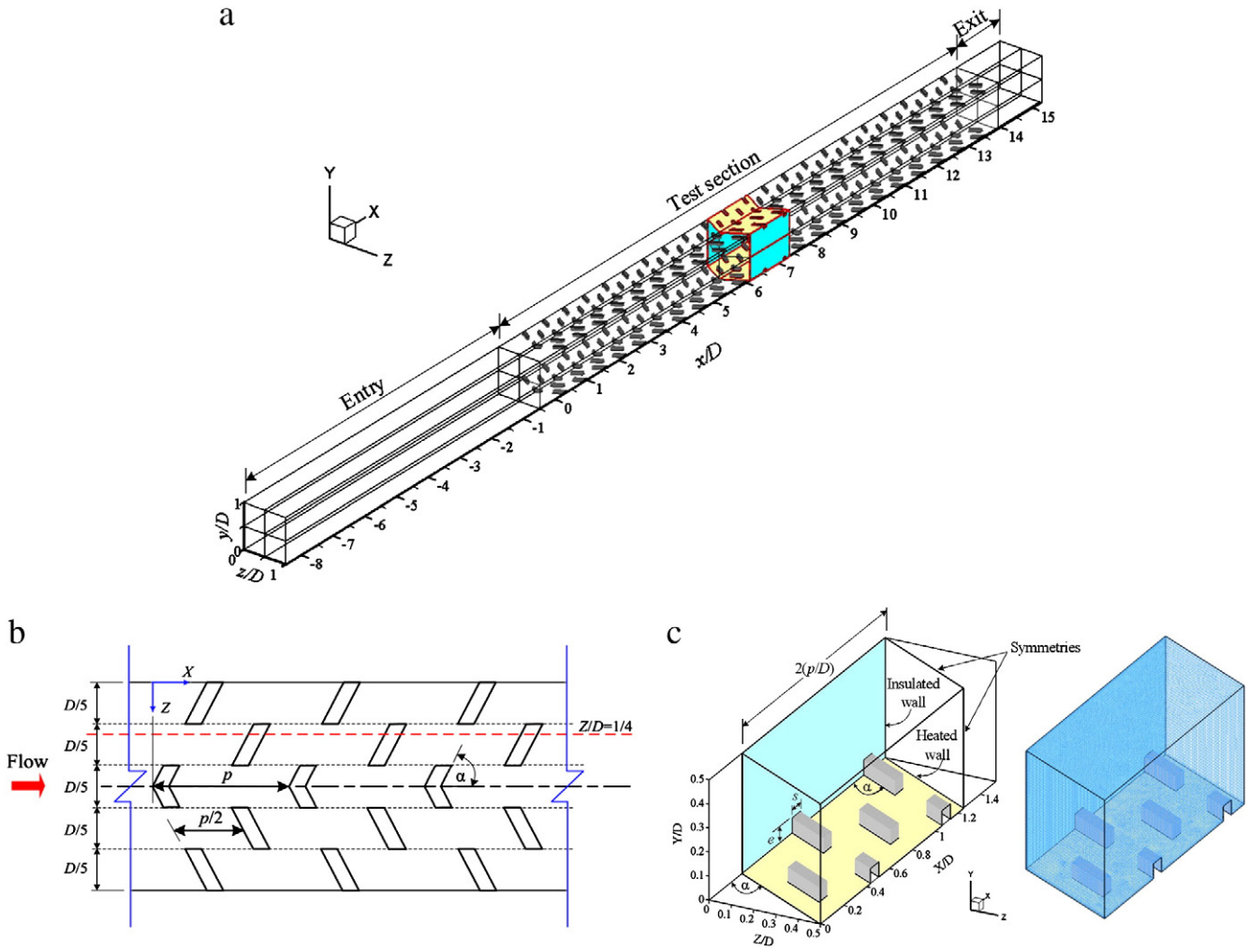

Fig. 1. (a) Duct geometry (b) plan view of periodic flow duct and (c) computational domain and grids.

The Reynolds-averaged approach to turbulence modeling requires that the Reynolds stresses, $-\rho\overline{u_i'u_j'}$ in Eq. (2) need to be modeled. The Boussinesq hypothesis relates the Reynolds stresses to the mean velocity gradients as seen in the equation below:

$$-\rho\overline{u_i'u_j'} = \mu_t\left(\frac{\partial u_i}{\partial x_j} + \frac{\partial u_j}{\partial x_i}\right) - \frac{2}{3}\left(\rho k + \mu_t\frac{\partial u_i}{\partial x_i}\right)\delta_{ij} \tag{5}$$

where k is the turbulent kinetic energy, as defined by $k = \frac{1}{2}\overline{u_i'u_i'}$, and δ_{ij} is the Kronecker delta. An advantage of the Boussinesq approach is the relatively low computational cost associated with the computation of the turbulent viscosity, μ_t given as $\mu_t = \rho C_\mu k^2/\varepsilon$. The RNG k–ε model is an example of the two-equation models that use the Boussinesq hypothesis. The RNG k–ε model is derived from the instantaneous Navier–Stokes equations using the "renormalization group" (RNG) method. The steady state transport equations are expressed as:

$$\frac{\partial}{\partial x_i}(\rho k u_i) = \frac{\partial}{\partial x_j}\left(\alpha_k\mu_{eff}\frac{\partial k}{\partial x_j}\right) + G_k - \rho\varepsilon \tag{6}$$

$$\frac{\partial}{\partial x_i}(\rho\varepsilon u_i) = \frac{\partial}{\partial x_j}\left(\alpha_\varepsilon\mu_{eff}\frac{\partial \varepsilon}{\partial x_j}\right) + C_{1\varepsilon}\frac{\varepsilon}{k}G_k - C_{2\varepsilon}\rho\frac{\varepsilon^2}{k} - R_\varepsilon. \tag{7}$$

In the above equations, α_k and α_ε are the inverse effective Prandtl numbers for k and ε, respectively. $C_{1\varepsilon}$ and $C_{2\varepsilon}$ are constants. The effective viscosity μ_{eff} is written by

$$\mu_{eff} = \mu + \mu_t = \mu + \rho C_\mu\frac{k^2}{\varepsilon} \tag{8}$$

where C_μ is a constant and set to 0.0845, derived using the RNG theory.

All the governing equations were discretized by the QUICK numerical scheme, decoupling with the SIMPLE algorithm and solved using a finite volume approach [18]. For closure of the equations, the RNG k–ε model was used in the present study. The solutions were converged when the normalized residual values were less than 10^{-5} for all variables but less than 10^{-9} only for the energy equation.

There are four parameters of interest in the present work, namely, the Reynolds number, friction factor, Nusselt number and thermal performance enhancement factor. The Reynolds number is defined as

$$\mathrm{Re} = \rho u_0 D/\mu\cdot \tag{9}$$

The friction factor, f is computed by pressure drop, ΔP across the length of the periodic duct, p as

$$f = \frac{(\Delta P / p)D}{2\rho u_0^2}. \tag{10}$$

The local heat transfer is measured by the local Nusselt number which can be written as

$$Nu_x = \frac{h_x D}{k_a}. \tag{11}$$

The area-average Nusselt number can be obtained by

$$Nu = \frac{1}{A}\int Nu_x dA. \tag{12}$$

The thermal performance enhancement factor (*TEF*) is defined as the ratio of the heat transfer coefficient of an augmented surface, h to that of a smooth surface, h_0, at an equal pumping power and given by

$$TEF = \frac{h}{h_0}\Big|_{pp} = \frac{Nu}{Nu_0}\Big|_{pp} = (Nu/Nu_0)/(f/f_0)^{1/3} \tag{13}$$

where Nu_0 and f_0 stand for Nusselt number and friction factor for the smooth duct, respectively.

3.1. Grid independence

The computational domain is resolved by regular Cartesian elements. A grid independence procedure was implemented by using the Richardson extrapolation technique over grids with different numbers of cells, 214,593 and 427,644. It is found that the variation in Nu and f values for the inline 60° V-discrete square rib at $BR = 0.0625$ and $Re = 15{,}000$ is marginal when increasing the number of cells from 214,593 to 427,644. Hence, there is no such advantage in increasing the number of cells beyond this value. Considering both convergent time and solution precision, the grid system of 214,593 cells was adopted for the current computation. For a full length duct, similar grid density was applied.

3.2. Boundary conditions

For a full length ribbed duct, a uniform velocity is introduced at the inlet while a pressure outlet condition is applied at the exit. For a periodic flow module, periodic boundaries are used for the inlet and outlet of the flow domain and a constant mass flow rate of air with 300 K ($Pr = 0.707$) is assumed in the flow direction. The physical properties of the air have been assumed to remain constant at initial air temperature. Impermeable boundary and no-slip wall conditions have been implemented over the duct walls as well as the rib surface apart from the enhanced wall treatment. The constant heat flux of two opposite heated walls is maintained at 2.5 kW/m^2 while the rib is assumed at adiabatic wall (high thermal resistance) conditions.

4. Results and discussion

4.1. Validation

Verification of the heat transfer and friction factor of the smooth square duct with no rib is first performed by comparing with the values from previous correlations under a similar operating condition as shown in Fig. 2. The present numerical smooth duct result is found to be in excellent agreement with correlation solutions obtained from the open literature [19] for both the Nusselt number and the friction factor, within ±5.3 and ±4.8% maximum deviations, respectively.

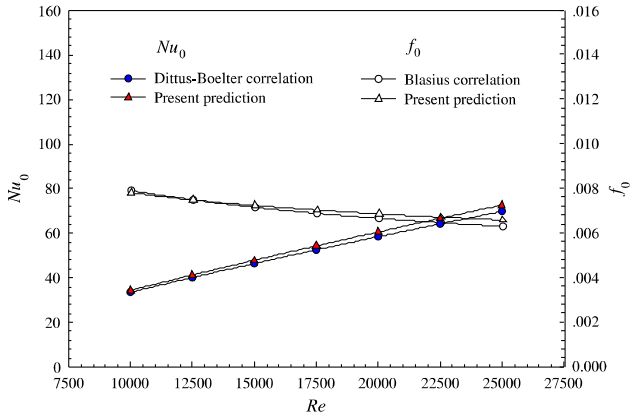

Fig. 2. Verification of (a) Nusselt number and (b) friction factor for smooth square duct.

The correlations of the Nusselt number and friction factor for turbulent duct flows with constant heat fluxed conditions are as follows:

Correlation of Dittus–Boelter,

$$Nu_0 = 0.023Re^{0.8}Pr^{0.4}. \quad \text{for} \quad \text{Re} \geq 10{,}000 \tag{14}$$

Correlation of Blasius,

$$f_0 = 0.079Re^{-0.25} \quad \text{for} \quad \text{Re} \leq 20{,}000 \tag{15a}$$

$$f_0 = 0.046Re^{-0.2} \quad \text{for} \quad \text{Re } b > N\, 20{,}000 \tag{15b}$$

Fig. 3 shows a comparison between the axial Nusselt number ratio, Nu_x/Nu_0, distribution predicted by the RNG k–ε model with various numerical schemes and measurements of SriHarsha et al. [9] at location, $Z/D = 1/4$ and $Re = 15{,}000$. In the figure, it is visible that the predicted Nu distributions are in excellent agreement with the measurement except for the area near the rib. The predicted results by higher-order numerical schemes, the second-order upwind scheme (SOU) and QUICK, are similar and agree well with measurements while the first-order upwind scheme (FOU) provides an under-predicted result, indicating that the use of FOU should be avoided. The axial Nu_x/Nu_0 profile prediction shows an undershooting in the middle region between the main V-rib and the discrete rib and an overshooting before reaching the discrete rib. Following the discrete rib, the predicted Nu_x/Nu_0 profile is dropped sharply in a small region behind the rib and then mimics the measurement very well until

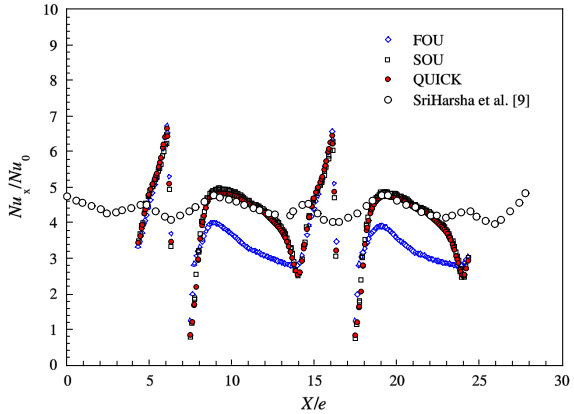

Fig. 3. Comparison between predicted Nu_x/Nu_0 and measured data for various numerical schemes at $Z/D = 1/4$, $Re = 15{,}000$.

entering the middle region again to complete the module. A close examination reveals that the areas of overshooting and undershooting are the areas of impingement/reattachment and separation flows, respectively while the measurement cannot capture both trends in these regions. It can be observed that the undershooting and overshooting levels are nearly the same leading to the predicted average Nu/Nu_0 of 3.6 while the measured Nu/Nu_0 is 3.9. Thus, the prediction deviation is found to be about 7.4% lesser. For pressure loss, the predicted f/f_0 value across the full length duct is 7.3 while the measured f/f_0 of SriHarsha et al. [9] is 7 for $Re=15{,}000$. Therefore, the discrepancy of the predicted f/f_0 values is around 4.3% higher than measured data. Therefore, it is noted that the numerical results are slightly under-predicted for the heat transfer but over-predicted for the friction loss in comparison with measurements.

4.2. Fully developed periodic condition

Understanding of a fully developed periodic profile condition in the ribbed duct is needed before discussing the results. The fully developed periodic flow and heat transfer conditions in the duct mounted repeatedly with inline 60° V-discrete ribs can be displayed by considering the axial Nu_x/Nu_0 and u/u_0 distribution plots as depicted in Fig. 4a to c. Here the Nu_x/Nu_0 and u/u_0 distributions of a full length ribbed duct and a periodic ribbed duct are presented all at $Z/D=1/4$ for $Re=10{,}000$ and $PR=0.625$.

Fig. 4a and b shows the axial Nu_x/Nu_0 distributions at $Z/D=1/4$ for the V-discrete ribs with $BR=0.0625$ and 0.125, respectively. In the figure, it is interesting to note that the axial Nu_x/Nu_0 profile appears to be periodic at the 2nd module and then, gradually increases to become a fully developed periodic profile at the 19th module or at $x/D\approx11.5$. This indicates that after the 19th module or $x/D\approx11.5$, the concept of fully developed periodic heat transfer condition is valid due to a constant Nu periodic profile throughout. Scrutinizing Fig. 4a and b reveals that when the rib height is increased from $BR=0.0625$ to 0.125, the axial Nu_x/Nu_0 value increases faster and is peak at the 9th module ($x/D\approx5$) before reducing to a constant periodic value at the 12th module or at $x/D\approx7$. However, the Nu_x/Nu_0 profile for the rib with $BR=0.0625$ provides the maximum value at the 14th module or at $x/D\approx8.5$.

Fig. 4c displays the axial u/u_0 profile along the tested duct for the V-discrete ribs with both $BR=0.0625$ and 0.125. It is seen in the figure that the u/u_0 profile for the $BR=0.125$ rib at $y/D=0.1875$ and $Z/D=1/4$ becomes periodic at the 2nd module and tends to increase to be fully developed periodic flow at the 12th module or at $x/D\approx7$, similar to the periodic heat transfer condition. However, for the rib with $BR=0.0625$ at $y/D=0.125$ and 0.1875, the u/u_0 profile also appears to be periodic at the 2nd module and gradually increases to become a fully developed periodic flow around the 17th module (or $x/D\approx10$ or 11). This means that the increase in rib height can induce quickly the secondary flow to be a fully developed periodic flow. In the present study, the periodic heat transfer is found to be a fully developed profile faster than the periodic flow. Therefore, the concept of fully developed periodic flow and heat transfer profiles can be applied efficiently to turbulent duct flow through ribs if the test duct is sufficiently long. It can be observed that the mean u/u_0 value in a developing periodic flow region is much lower than that in a fully developed one while the average Nu_x/Nu_0 is not much different for both the periodic regions. Again, with considering both convergent time and solution precision, only a fully developed periodic flow and heat transfer duct model is employed in the next computation.

4.3. Effect of rib thickness

In order to investigate the rib thickness effect on flow and thermal characteristics, the V-discrete square ribs with $s/D=0.0625$ are replaced by the thin ribs with $s/D=0.0125$ on a fully developed periodic flow and heat transfer duct model as shown in Fig. 5a and b

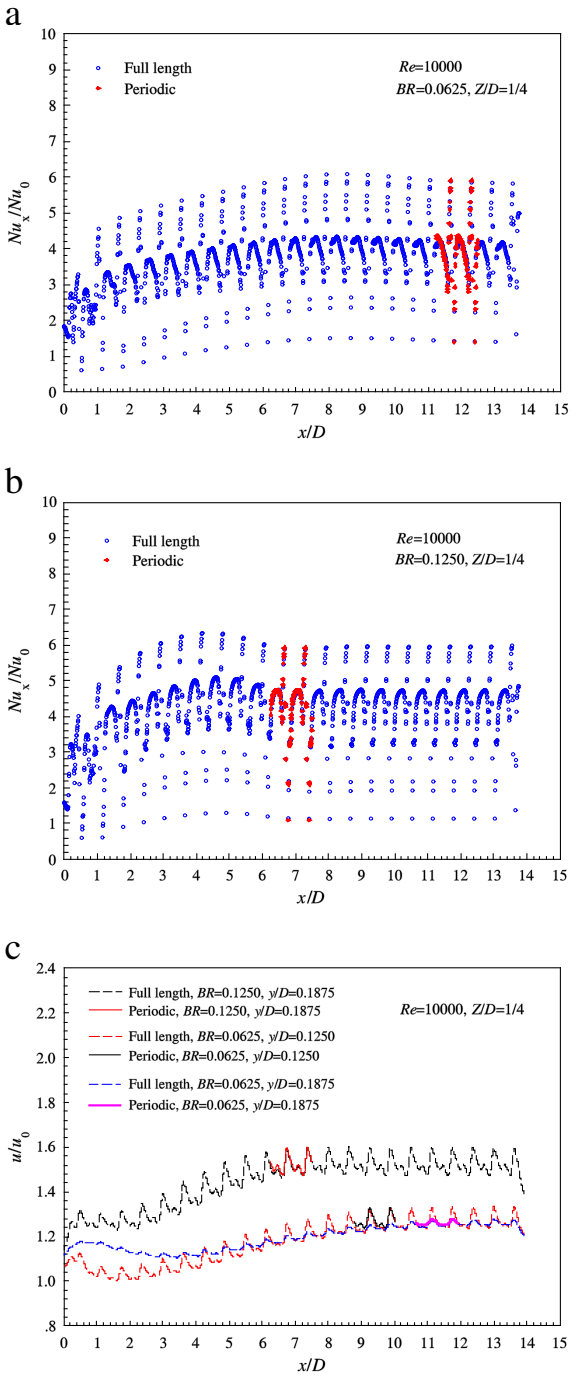

Fig. 4. Axial distributions of (a) Nu_x/Nu_0 for $BR=0.0625$, (b) Nu_x/Nu_0 for $BR=0.125$ and (c) u/u_0 at various locations for $Re=10{,}000$, and $PR=0.625$.

for the square and thin rib ducts, respectively. In the figure, the periodic flow duct consisting of 2 modules at which a single module considered herein begins at $X/p=0$ and ends at $X/p=1$ where p is pitch spacing distance between the consecutive ribs and set to $10e$ (or $PR=0.625$). Both the ribs have the same height, $BR=0.0625$ and are mounted repeatedly on the upper and lower heated walls only while sidewalls are insulated. Please keep in mind that the V-broken square rib with orientation, pitch and height mentioned above provides the best thermal performance [4,9].

The local Nu_x contour for the lower duct wall fitted with the inline 60° V-discrete ribs with $BR=0.0625$ and $PR=0.625$ at $Re=15{,}000$ is presented in Fig. 6a and b for the square and thin ribs, respectively. In the figure, it is apparent that the higher Nu_x values over the lower wall

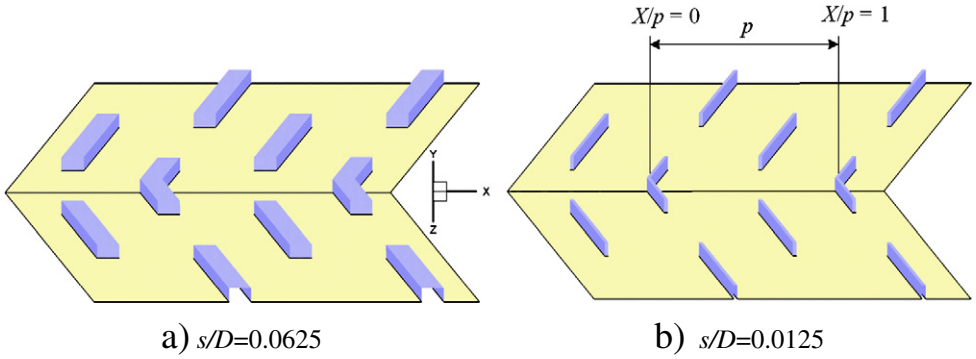

Fig. 5. Arrangement of V-discrete (a) square and (b) thin ribs on lower wall.

are seen to be in larger areas, especially in the vicinity of the V-rib and discrete-rib elements while the lower Nu_x is found in a region around the rib element near the sidewalls. The peak Nu_x values are observed at the impingement flow areas on the wall in front of the V-rib and the discrete-rib elements. In scrutiny of the square and thin ribs, it is visible that the higher Nu_x values of the thin rib appear to be in larger region than those of the square one. This is because the use of the thin rib can induce larger recirculation or vortex flow appearing behind the rib than that of the square rib as can be seen from the streamline plots in Fig. 6. Therefore, it is expected that the thin rib should provide higher heat transfer than the square one. The peak Nu_x values for both the V-discrete ribs are found to be about 5 times above those for the smooth duct with no rib. This indicates a merit of using the ribs over the smooth duct for enhancing heat transfer.

The variation of the average Nu/Nu_0 and f/f_0 values with Reynolds numbers for the V-discrete square and thin ribs at $BR = 0.0625$ is depicted in Fig. 7a and b, respectively. In the figure, it is worth noting that the Nu/Nu_0 value tends to slightly decrease with the rise of Reynolds number while the f/f_0 shows an opposite trend. The Nu/Nu_0 value for the thin rib is seen to be higher than that for the square one at about 5% depending on Re values while the f/f_0 value for the thin rib is some 17% above that for the square one. Thus, the vortex induced impingement flow (see Fig. 6) due to the V-discrete ribs as well as the role of better flow mixing brings in the augmentation of heat transfer from the duct wall. In addition, it can be noted that the V-discrete ribs provide higher Nu value than the smooth duct at all Re values. The scrutiny of Fig. 7 reveals that the duct with thin rib provides the heat transfer rate and friction factor of about 3.0–3.7 and 9.0–10.5 times over the duct with no rib, respectively, depending on the Re values. Although the square rib yields lower friction loss, the thin rib is still in more consideration because of higher Nu value. Thus, the next section will focus on the thin rib only.

4.4. Flow structure of thin rib

The flow structure in the duct mounted repeatedly with the inline 60° V-discrete thin rib can be displayed by considering the velocity vector and temperature field plots in transverse planes for $Re = 15{,}000$ in a lower half module as depicted in Fig. 8 at various axial locations, $X/p = 0$, 0.2 (see $X/p = 1.2$ in the figure), 0.4 (see $X/p = 2.4$), 0.6 and 0.8 (see $X/p = 1.8$), respectively. The velocity vectors and temperature fields in transverse planes are the most notable characteristics of the effects of the V-discrete rib on the mainstream flow. These effects are: mainstream flow separation, recirculation/vortex, and secondary flow. It is visible that two counter-rotating vortices or longitudinal vortex flows caused by the rib appear on the lower part of duct. The appearance of the longitudinal vortex flows can help to increase higher the heat transfer in the duct because of transporting the fluid from the core to the near wall regimes.

4.5. Effect of blockage ratio, BR

Fig. 9a and b displays the variation of the average Nu/Nu_0 ratio and friction factor ratio, f/f_0 with different BRs of the V-discrete ribs at $PR = 0.625$ and various Re values, respectively. It is noted that both the Nu/Nu_0 and f/f_0 values tend to increase with the rise of BR values. This can be attributed to the fact that increasing the rib height can induce a larger recirculation zone behind the rib leading to higher vortex

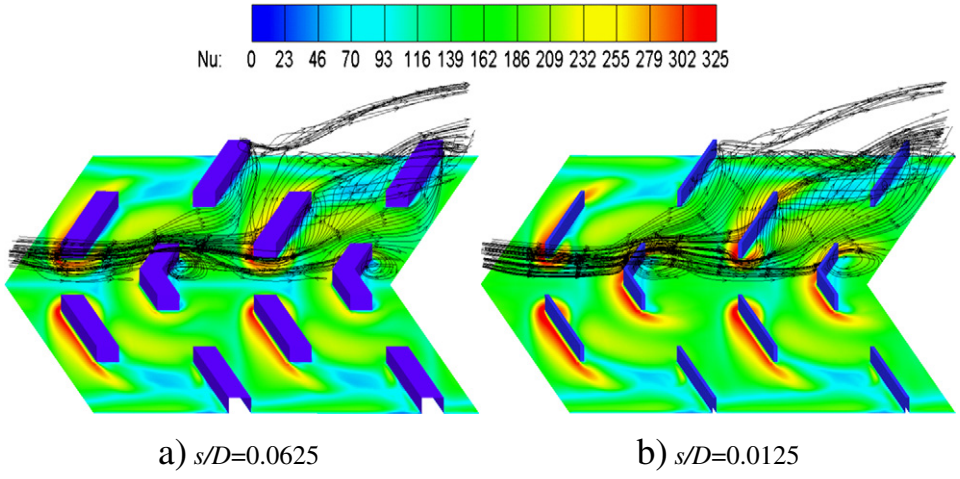

Fig. 6. Streamlines and Nu_x contours for V-discrete (a) square and (b) thin ribs at $Re = 15{,}000$.

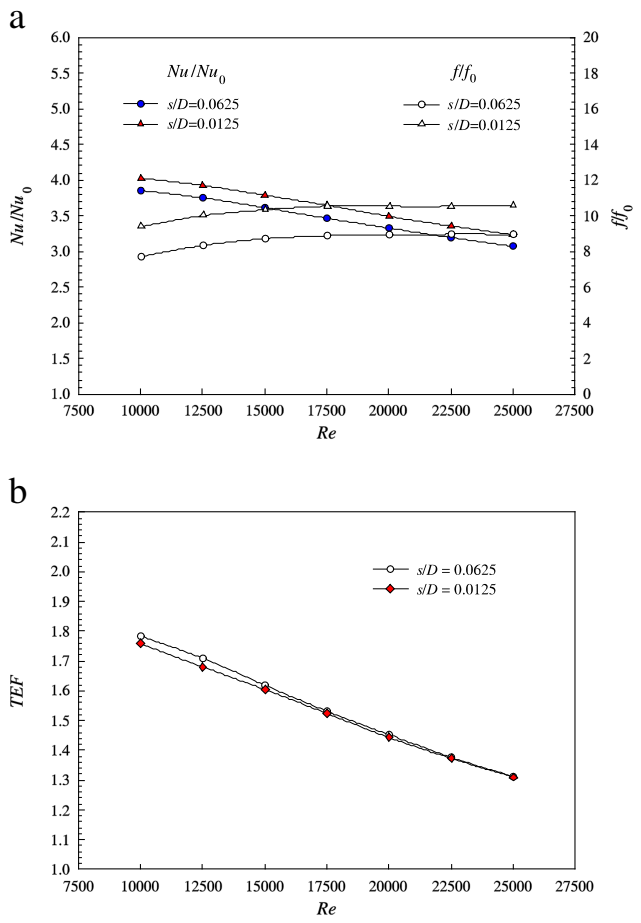

Fig. 7. Variation of (a) Nu/Nu_0 and f/f_0, and (b) *TEF* with Reynolds number for thin and square ribs.

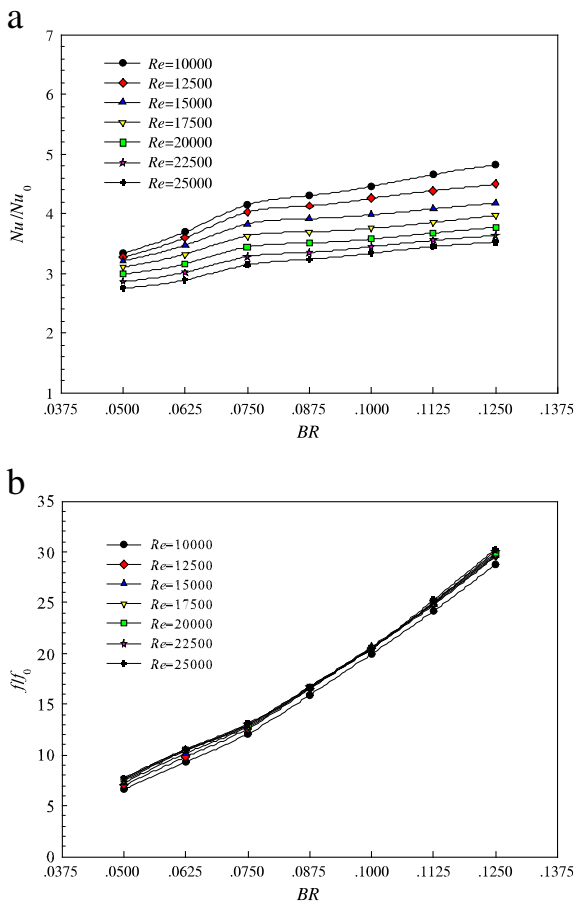

Fig. 9. Variation of (a) Nu/Nu_0 and (b) f/f_0 with Reynolds number for various *BR*s.

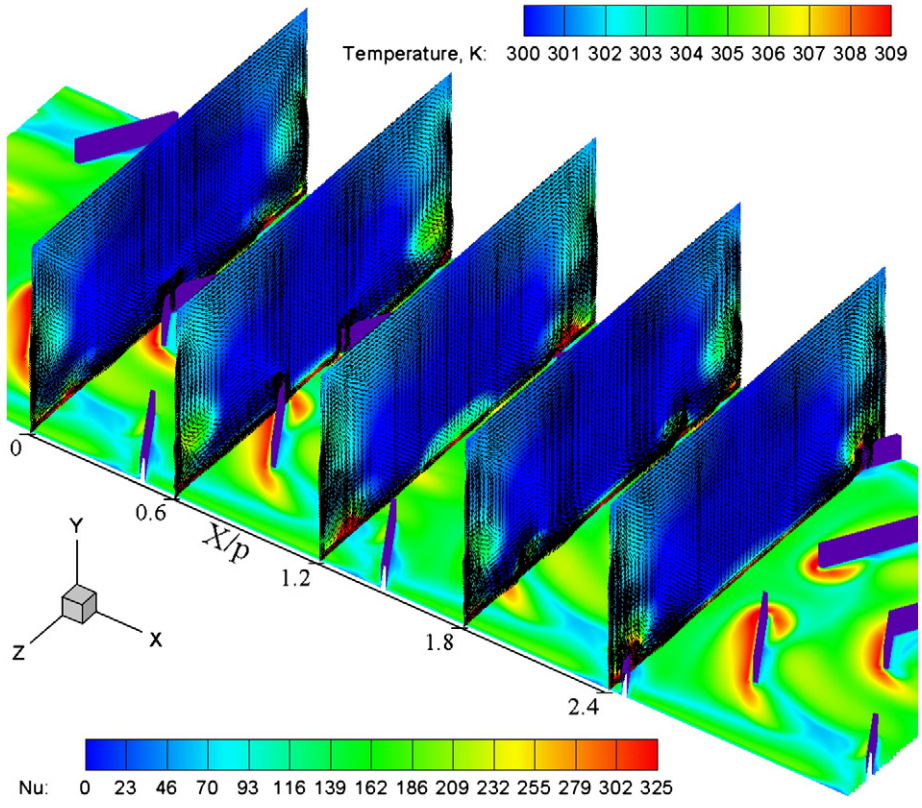

Fig. 8. Velocity vectors and temperature contours in transverse planes at $Re = 15{,}000$.

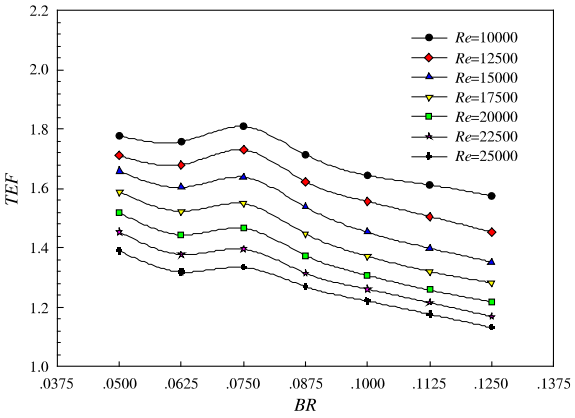

Fig. 10. Effect of *BR*s on *TEF*.

strength and turbulence intensity of the flow, enhancing the heat transfer and pressure drop. The Nu/Nu_0 shows a decrease trend with increasing the *Re* while the f/f_0 is nearly independent, especially for higher *Re* value. The rib with $BR=0.125$ gives the highest Nu/Nu_0 and f/f_0 while the one with $BR=0.05$ provides the lowest. The *Nu* and *f* values for the duct with ribs appear to be about 2.7–4.7 and 6.5–29.5 times above those for the duct with no rib, depending on the *BR* and *Re* values. Closer inspection reveals that for $BR>0.075$, the gradient of Nu/Nu_0 tends to decrease while that of f/f_0 shows a steeper increase.

Fig. 10 shows the variation of the *TEF* value for the V-discrete ribbed square duct. It is visible that the *TEF* tends to decrease with the rise in *BR* and *Re* values for $BR>0.075$. The rib with $BR=0.075$ provides the highest *TEF* of about 1.81 at the lowest *Re* but the one with $BR=0.05$ yields the highest *TEF* for $Re>15{,}000$. The *TEF* of the rib is seen to vary between 1.13 and 1.81, depending on the *BR* and *Re* values, indicating higher thermal performance over the smooth duct with no rib.

5. Conclusions

Turbulent periodic flow and thermal characteristics in a square duct mounted repeatedly with inline 60° V-discrete ribs are investigated numerically. The ribbed duct flow is found to be fully developed periodic flow and heat transfer profiles at about $x/D=7$–11 downstream of the inlet. The P-vortex flow caused by the rib helps to induce impingement flows on the duct wall leading to greater increase in the heat transfer rate. The heat transfer in the duct with the ribs is about 200−370% higher than the smooth duct with no rib. However, the heat transfer augmentation is related to the enlarged friction loss ranging from 8 to 10.5 times above the smooth duct. Both the thin and square ribs provide nearly similar thermal performance while the thin rib yields higher *Nu* and *f* values. The *TEF* for the V-discrete thin rib is much higher than unity and its maximum value is about 1.8 at $BR=0.075$. The heat transfer rate for the rib with $BR=0.075$ is 3 − 4 fold above that for the smooth duct while the friction factor is about 12 − 13 times.

References

[1] R.L. Webb, E.R.G. Eckert, R.J. Goldstein, Heat transfer and friction in tubes with repeated-rib roughness, International Journal of Heat and Mass Transfer 14 (1971) 601–617.
[2] J.C. Han, Y.M. Zhang, C.P. Lee, Augmented heat transfer square channels with parallel, crossed, and V-shaped ribs, ASME Journal of Heat Transfer 113 (1991) 590–596.
[3] S.C. Lau, R.T. Kukreja, R.D. McMillin, Effects of V-shaped rib arrays on turbulent heat transfer and friction of fully developed flow in a square channel, International Journal of Heat and Mass Transfer 34 (7) (1991) 1605–1616.
[4] J.C. Han, Y.M. Zhang, High performance heat transfer ducts with parallel broken and V-shaped broken ribs, International Journal of Heat and Mass Transfer 35 (1992) 513–523.
[5] P.R. Chandra, C.R. Alexander, J.C. Han, Heat transfer and friction behavior in rectangular channels with varying number of ribbed walls, International Journal of Heat and Mass Transfer 46 (2003) 481–495.
[6] P. Promvonge, C. Thianpong, Thermal performance assessment of turbulent channel flows over different shaped ribs, International Communications in Heat and Mass Transfer 35 (10) (2008) 1327–1334.
[7] G. Tanda, Heat transfer in rectangular channels with transverse and v-shaped broken ribs, International Journal of Heat and Mass Transfer 47 (2004) 229–243.
[8] S.Y. Won, P.M. Ligrani, Comparisons of flow structure and local Nusselt numbers in channels with parallel- and crossed-rib turbulators, International Journal of Heat and Mass Transfer 47 (2004) 1573–1586.
[9] V. Sri Harsha, S.V. Prabhu, R.P. Vedula, Influence of rib height on the local heat transfer distribution and pressure drop in a square channel with 90° continuous and 60° V-broken ribs, Applied Thermal Engineering 29 (11–12) (2009) 2444–2459.
[10] P. Promvonge, Heat transfer and pressure drop in a channel with multiple 60° V-baffles, International Communications in Heat and Mass Transfer 37 (2010) 835–840.
[11] A. Gupta, V. SriHarsha, S.V. Prabhu, R.P. Vedula, Local heat transfer distribution in a square channel with 90° continuous, 90° saw tooth profiled and 60° broken ribs, Experimental Thermal and Fluid Science 32 (2008) 997–1010.
[12] K. Tatsumi, H. Iwai, K. Inaoka, K. Suzuki, Numerical analysis for heat transfer characteristics of an oblique discrete rib mounted in a square duct, Numerical Heat Transfer Part A: Applications 44 (8) (2003) 811–831.
[13] Y.T. Yang, C.W. Hwang, Numerical calculations of heat transfer and friction characteristics in rectangular ducts with slit and solid ribs mounted on one wall, Numerical Heat Transfer Part A: Applications 45 (4) (2004) 363–375.
[14] K.Y. Kim, Y.M. Lee, Design optimization of internal cooling passage with V-shaped ribs, Numerical Heat Transfer Part A: Applications 51 (11) (2007) 1103–1118.
[15] P. Promvonge, S. Kwankaomeng, Periodic laminar flow and heat transfer in a channel with 45° staggered V-baffles, International Communications in Heat and Mass Transfer 37 (2010) 841–849.
[16] P. Promvonge, S. Sripattanapipat, S. Kwankaomeng, Laminar periodic flow and heat transfer in square channel with 45° inline baffles on two opposite walls, International Journal of Thermal Sciences 49 (2010) 963–975.
[17] P. Promvonge, W. Jedsadaratanachai, S. Kwankaomeng, Numerical study of laminar flow and heat transfer in square channel with 30° inline angled baffle turbulators, Applied Thermal Engineering 30 (2010) 1292–1303.
[18] S.V. Patankar, Numerical Heat Transfer and Fluid Flow, McGraw-Hill, New York, 1980.
[19] F. Incropera, P.D. Dewitt, Introduction to Heat Transfer, 5 rd edition, John Wiley & Sons Inc, 2006.